Supplementary Information

Protonic Ceramic Electrochemical Cells for Hydrogen Production and Electricity Generation: Exceptional Reversibility, Stability, and Demonstrated Faradaic Efficiency

Sihyuk Choi[a,b], Timothy C. Davenport[a], Sossina M. Haile*[a]

[a] *Materials Science and Engineering, Northwestern University, Evanston, IL, USA*
[b] *Department of Mechanical Engineering, Kumoh National Institute of Technology, Gyeongbuk 39177, Republic of Korea*

correspondence to: sossina.haile@northwestern.edu (S.M.H)

This PDF file includes:

Experimental procedure

Air electrode preparation

Powders of $PrBa_{0.5}Sr_{0.5}Co_{1.5}Fe_{0.5}O_{5+\delta}$ (PBSCF), $Sm_{0.5}Sr_{0.5}CoO_{3-\delta}$ (SSC), $La_{0.6}Sr_{0.4}Co_{0.2}Fe_{0.8}O_{3-\delta}$ (LSCF), and $La_{0.8}Sr_{0.2}MnO_3$ (LSM) were synthesized *via* a variant of the Pechini process in which nitrate precursors are dissolved in aqueous solution using citric acid and ethylene glycol as complexing agents.[1] The black char resulting from the gelation and drying steps was calcined at 600 °C for 4 h to eliminate organic residue. The calcined powders were ball milled, then sintered at 1150 °C for 12 h (PBSCF), 1200 °C for 12 h (SSC), 1200 °C for 12 h (LSCF), and 1450 °C for 5 h (LSM), to achieve single phase products as confirmed by X-ray diffraction (XRD) (Scintag XDS2000, Cu Kα radiation, 40 kV, 20 mA).

Conventional cell preparation

The fuel electrode-supported cells with the configuration of NiO-BZCYYb4411/BZCYYb4411/air electrode configuration were fabricated using a drop-coating method. The composite fuel electrode was formed from in-house synthesized NiO and BZCYYb4411 electrolyte powders, the former by the glycine nitrate process, and the latter by typical solid state reaction method. For NiO synthesis, nickel nitrate (Sigma Aldrich) was dissolved in distilled water and glycine (98.5%, Sigma Aldrich) was added in the solution in a 1:1 molar ratio. The solution was heated on a hot plate set at 350 °C to evaporate water, yielding a viscous liquid. Fine NiO powders were obtained via a subsequent combustion reaction. The resulting NiO powder was calcined at 800 °C for 4h in air. The $BaZr_{0.4}Ce_{0.4}Y_{0.1}Yb_{0.1}O_3$ (BZCYYb4411) electrolyte powder was prepared with stoichiometric quantities of barium carbonate (>99%, Sigma Aldrich), zirconium oxide (99.5%, Alfa Aesar), cerium oxide (99.9%, Alfa Aesar) and the oxides of the dopants, yttrium oxide (99.9%, Alfa Aesar), and ytterbium oxide (99.9%, Alfa Aesar). The mixture was first ball-milled for 24 h with yttria-stabilized zirconia balls (Inframat Advanced Materials, spherical 3.0 mm) using ethanol as the milling medium. After removing the ethanol *via* a drying step at 100 °C, the powder was lightly ground then calcined at 1100 °C for 10 h. The milling and calcination steps were repeated a second time to ensure phase formation. The NiO-BZCYYb4411 composite fuel electrode was prepared by ball milling NiO powder, BZCYYb4411 powders, and starch in a weight ratio of 65:35:0.5

in ethanol for 24 h. After a drying step, the composite powders were mechanically pressed into a disc and lightly sintered at 800 ^{o}C for 4 h.

A thin electrolyte layer was applied atop the porous anode by a drop coating technique. Specifically, the electrolyte powder was suspended in a multi-component organic fluid in a 1:10 solid-to-fluid weight ratio, where the fluid was comprised of a mixture of 2-butanol binder (Alfa Aesar), polyvinyl butyral (Tape Casting Warehouse, TCW), butyl benzyl phthalate (TCW), polyalkylene glycol (TCW), and triethanolamine (Alfa Aesar). After drop-coating onto the lightly fired support, the resulting fuel electrode/electrolyte bi-layer was heat-treated at 400 ^{o}C for 1 h to remove organics. Sintering was carried out immediately thereafter in a two-step protocol in which the sample was first exposed to 1550 ^{o}C for 5 min and then 1500 ^{o}C for 4 h to maximize grain growth while minimizing barium volatilization. The resulting electrolyte thickness was ~15 μm. The air electrode layer was applied in the form of a slurry, comprised of a mixture of air electrode powder and the organic binder, V-006 (Heraeus) in a 1:1.2 ratio. After slurry deposition onto the electrolyte layer, the complete cell was sintered at 950 ^{o}C for 4 h in air (PBSCF) and 1100 ^{o}C for 4 h (Both LSCF and LSM), resulting in ~20 μm thick with an effective area of 0.28 cm^2. The microstructures and morphologies were observed using a field emission scanning electron microscope (SEM) (Hitachi SU8030).

Cell preparation with pulsed laser deposition (PLD) layer

To facilitate PLD of PBSCF, large targets of the material were fabricated. Pre-calcined PBSCF powders were mechanically compacted into discs using a uniaxial press (20 MPa for 1 min), followed by high pressure in an isostatic press (~250 MPa for 20 min). Green bodies were sintered at 1150 ^{o}C for 12 h to yield compacts ~ 24 mm in diameter and 4-5 mm in thickness. Typical densities were ~95 % of theoretical, as determined by the Archimedes method. PBSCF films were grown on the electrolyte side of NiO+BZCYYb4411/BZCYYb4411 bi-layer cells using a PVD PLD/MBE 2300 in the Northwestern University PLD core facility. The substrate was heated at a rate of 30 °C/min and then held at 650 °C for growth. The oxygen pressure in the chamber was set at 30 mTorr. The growth rate was found to be 20.8 nm min^{-1} for the conditions employed (248 nm KrF laser, 270 mJ/pulse, 5 Hz repetition rate). Upon completion of the deposition, the chamber was vented to 300 Torr oxygen pressure (to facilitate oxidation) and cooled at a rate of 10 °C/min. As with the conventional cells, a slurry of PBSCF was then

brush-painted (now onto the PBSCF thin film rather than the electrolyte) and the complete cell was sintered at 950 °C for 4 hours in air.

Electrolysis and fuel cell measurement

Ag wires (GoodFellow) were attached at both electrodes of single cell using an Ag paste (SPI supplies) as a current collector. An alumina tube and a ceramic adhesive (Ceramabond 552, Aremco) were employed to fix and seal the single cell. For a typical experiment, humidified hydrogen (3 % H_2O) and humidified air (3 % H_2O) were supplied with a flow rate of 50 sccm of hydrogen and 200 sccm of air, using a water bubbler for humidification. Impedance spectra were recorded under open circuit voltage (OCV) in a frequency range of 100 kHz to 0.1 Hz with AC perturbation of 20 mV. *I-V* curves were collected using a BioLogic SP-300 Potentiostat at operating temperature from 500 to 650 °C in intervals of 50 °C. The current stability was measured under a fixed voltage of 1.3 V at 550 °C. For experiments varying the H_2O concentration in air, humidified air was supplied with concentrations of 3, 5, 7, and 10 % H_2O, achieved by varying the temperature of the water bubbler. For Faradaic efficiency tests, humidified hydrogen was replaced with 5 % H_2/Ar, and the flow rate fixed at 150 ml min^{-1} unless otherwise specified. The hydrogen concentration of the fuel electrode effluent was measured by an inline mass spectrometer (Pfeiffer Thermostar GSD301T2). The mass spectrometer was calibrated using a six-point calibration using known mixtures of hydrogen in Ar between 5 % H_2 and 15 % H_2 immediately before the experiment.

Electrochemical Characteristics of Mixed Conductors

Two mistakes are commonly encountered in the interpretation of the behavior of electrochemical cells based on mixed ion (proton) and electron conductors used in electrolysis. The first is in the interpretation of the impedance data. Most authors recognize that the high frequency ohmic resistance is $\lim_{\omega\to\infty}\{Z\} = R_{\text{ohmic}} = \frac{R_{e^-}R_{H^+}}{R_{H^+}+R_{e^-}}$, as given in Eq. (11) of the main text. That is, R_{ohmic} does not directly give the value of the ionic (protonic) resistance. In contrast, many misinterpret the meaning of the resistance in the D.C. limit and incorrectly take R_p to be ($R_{DC} - R_{\text{ohmic}}$). The true relationship of the resistance in the DC limit to the material properties

is, however, $\lim_{\omega\to 0}\{Z\} = R_{DC} = \frac{R_{e^-}\left(R_{H^+}+R_P\right)}{R_{e^-}+R_{H^+}+R_P}$, as given in Eq. (12) of the main text. Thus, the incorrect interpretation of R_{DC} underestimates R_P, just as an incorrect assumption that R_{ohmic} corresponds to the ionic resistance would underestimate R_{H^+}. In both cases, electronic leakage increases the measured conductance and such leakage must be accounted for in order to extract the true material properties.

The second common mistake is in the measurement of hydrogen production. Review of the literature reveals that many authors report hydrogen production from protonic ceramic cells to be zero under open circuit conditions. However, it is generally not possible to actually measure the hydrogen production as being zero. In the protonic ceramic system, hydrogen from electrolysis is generated at the fuel electrode, and thus the hydrogen content in the exhaust from this electrode must be measured. Typically, some amount of hydrogen (3 to 5%) is supplied to the fuel electrode, and thus even under open circuit conditions, hydrogen is detected in the exhaust stream. For a cell with no electronic leakage, it is appropriate to calibrate the system such that the detected hydrogen signal corresponds to the inlet hydrogen, meaning that the hydrogen production is zero. However, when the open circuit voltage is lower than the Nernst value due to electronic conductivity, there is, as discussed in the main text, a net *loss* of hydrogen at open circuit. Explicitly, combining Eqs. (8) and (13) text yields

$$I_{H^+}^{OC} = \frac{-V_{OC}}{R_{DC}}\left(1-\frac{V_{OC}}{V_N}\right)$$

Thus, taking the hydrogen signal to correspond to zero production at open circuit from an electronically leaky cell is simply incorrect. Doing so overestimates the hydrogen production at all conditions – at open circuit and, due to the incorrect calibration, also under bias. One cannot simultaneously attribute $V_{OC} < V_N$ to electronic leakage and take the hydrogen production at open circuit to be zero. These two conditions are contradictory. Yet, many authors report both to be true. Because there are fewer challenges to measuring voltage than hydrogen signal above an unquantified background, it is likely that the V_{OC} measurements are correct, whereas the hydrogen production values reported in these studies are overestimated. Consequently, Faradaic efficiencies are unlikely to be as high as many authors have suggested.

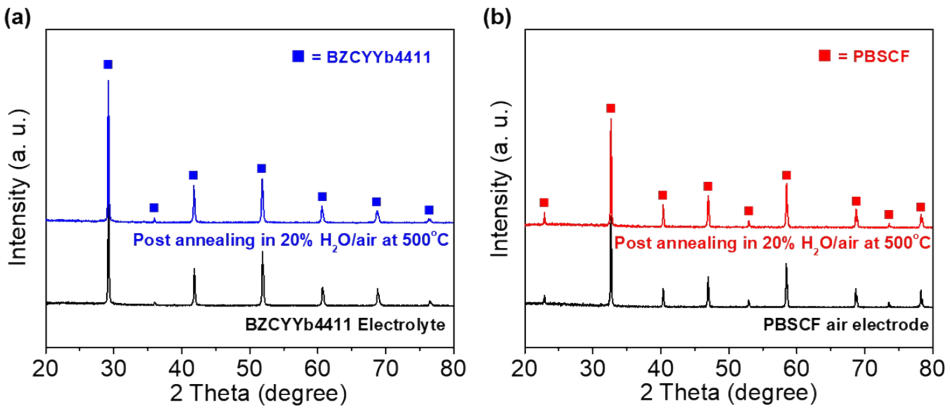

Figure S1. Steam tolerance of BZCYYb4411 electrolyte and PBSCF air electrode. X-ray diffraction patterns of (a) BZCYYb4411 electrolyte and (b) PBSCF air electrode (powder form) after treatment in 20 % H_2O-80 % air at 500 ^oC for 24 h.

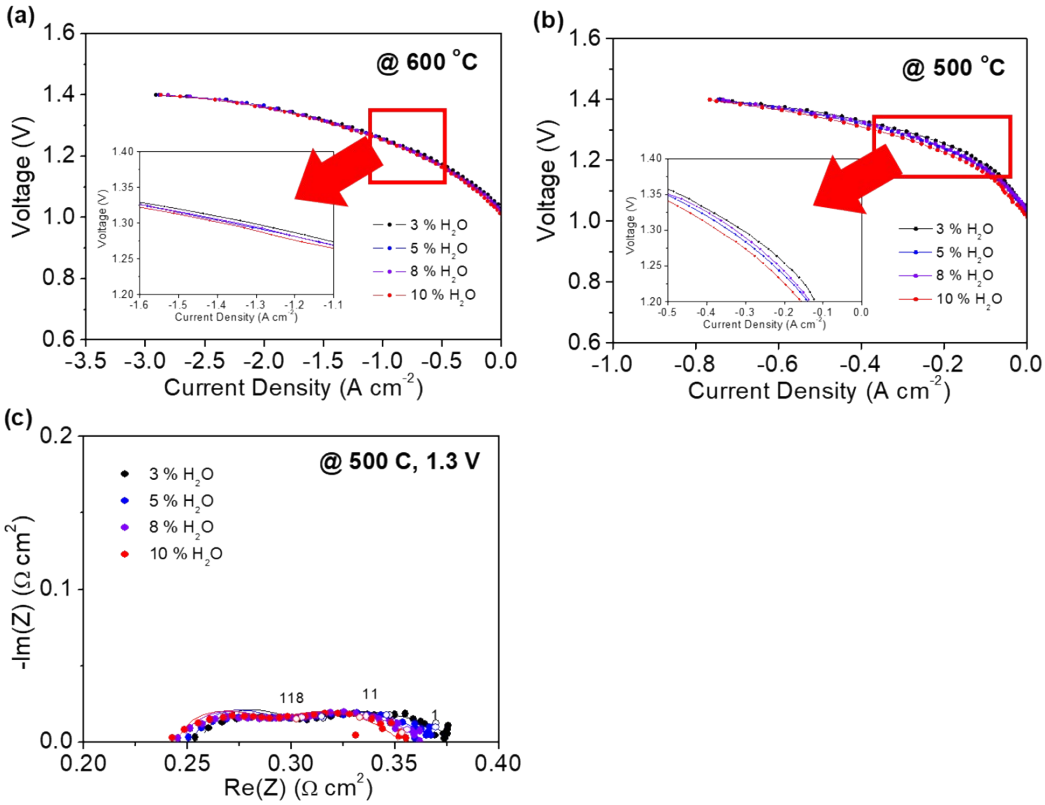

Figure S2. Electrochemical charateristics of various H_2O concentration. IV curves of the effect on various H_2O concentration for air electrode at (a) 600 °C and (b) 500 °C. (c) Nyquist impedance plots and the corresponding fit curves as function of H_2O concentration at 500 °C and 1.3 V.

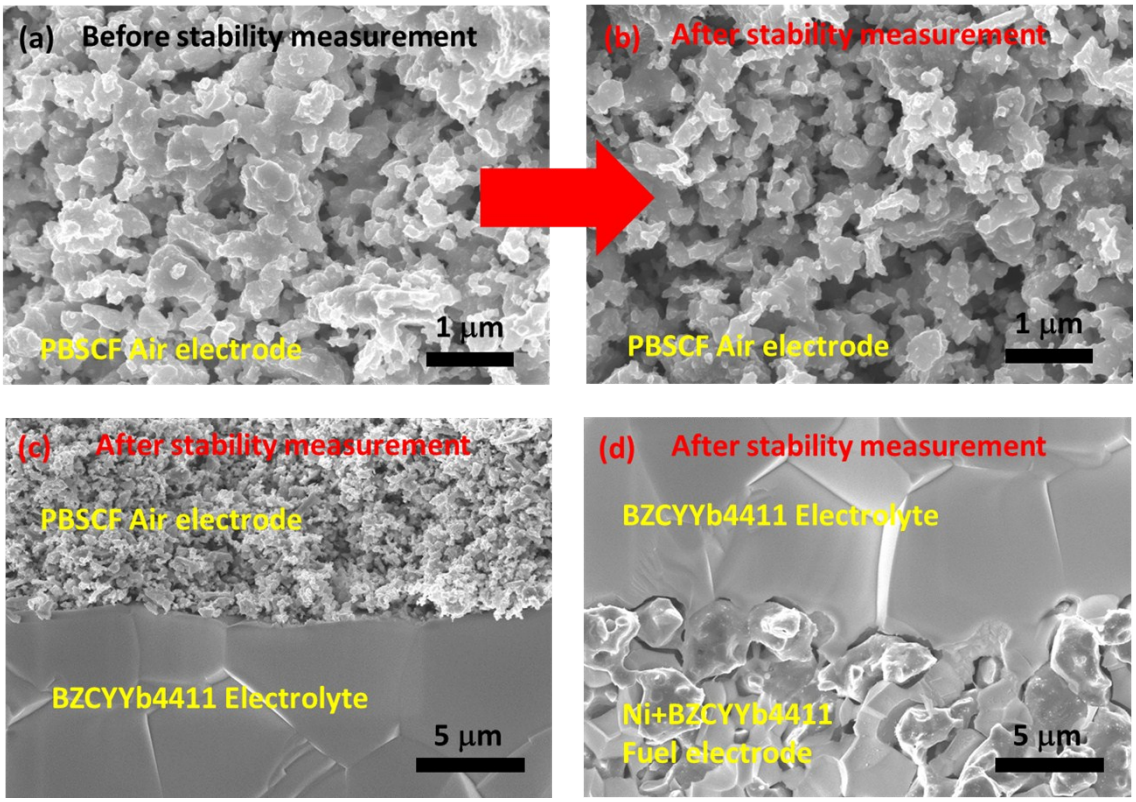

Figure S3. Absence of microstrucural changes during stability measurement with conventional cell. SEM images of electrochemical cell before and after stability measurement for 500 h. High-magnification images of air electrode morphologies (a) before and (b) after stability measurement. Cross-sectional images of the interfaces at (c) air electrode/electrolyte (d) fuel electrode/electrolyte after stability measurement. The dense electrolytes still well adhered to both electrode without any cracking or delamination.

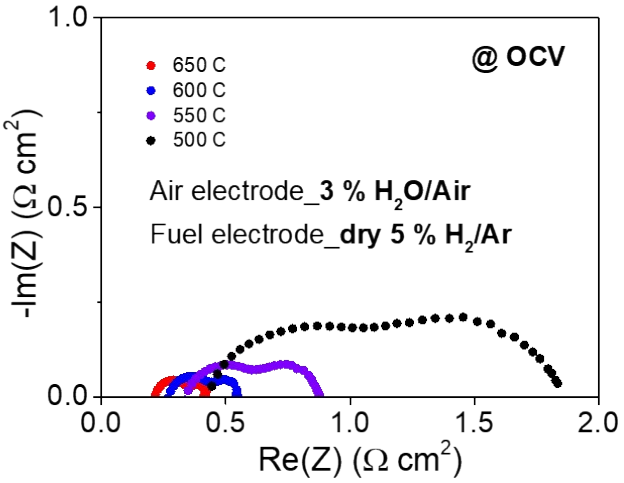

Figure S4. Impedance spectra of conventional cell under OCV condition at 600 °C. Dry 5 % H_2 (balanced in Ar) is supplied to the fuel electrode and humidified (3 % H_2O) air is fed to air electrode.

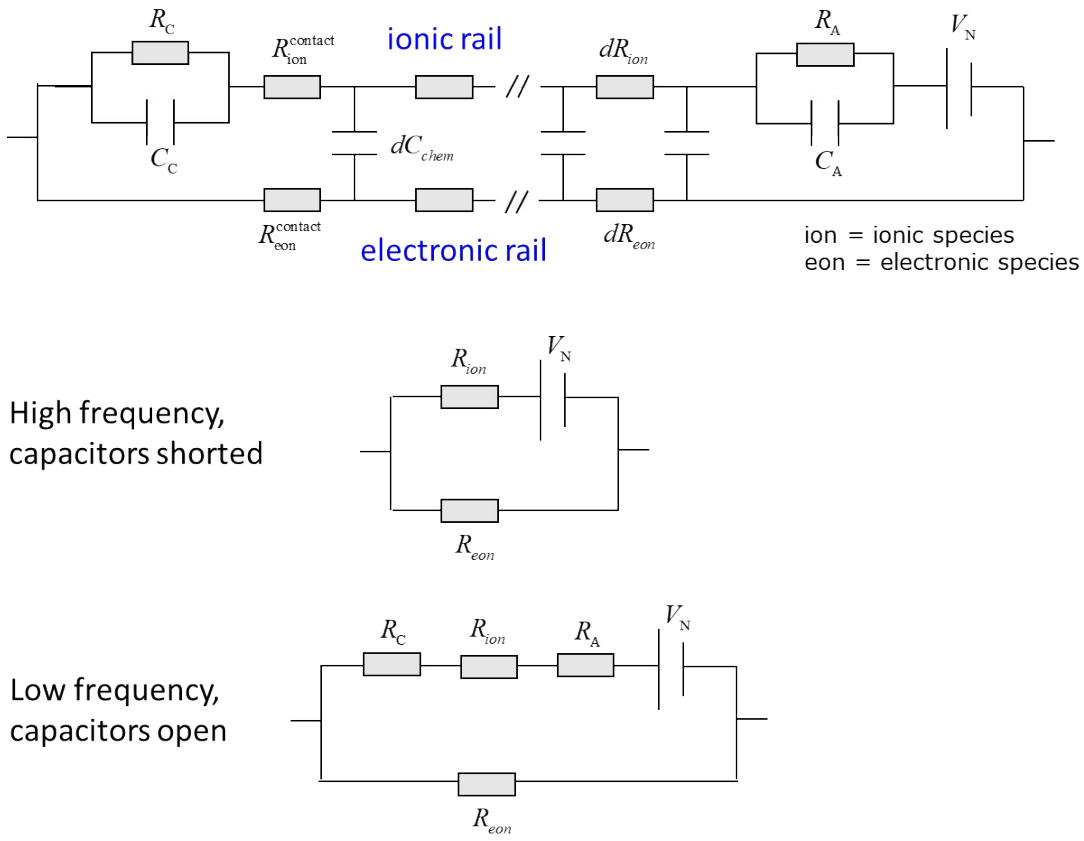

Figure S5. Simplified equivalent circuit representation of an electrochemical cell with a mixed ion and electron conducting electrolyte. Top: the circuit at frequencies below the bulk characteristic frequency, at which the dielectric capacitance of the electrolyte is effectively open and can be ignored. Ions and electrons move along parallel paths, and under the assumption of local electroneutrality, differential ionic and electronic resistances are linked by the differential chemical capacitance which ensures that changes in concentration of two types of species are balanced. R_C and R_A are, respectively, the cathode and anode electrochemical reaction resistances, which are accompanied by capacitance terms, C_C and C_A. In principle, non-conventional circuit elements are required to completely describe the impedance response, but such elements are omitted here for simplicity.[2,3] Middle: at high frequency, capacitors are shorted. Bottom: at low frequency, capacitors are open. R_{ion} in the middle and bottom circuits includes both the bulk ionic resistance and the ionic contact resistance of the top circuit. Similarly, R_{eon} includes both the bulk electronic resistance and the electronic contact resistance.

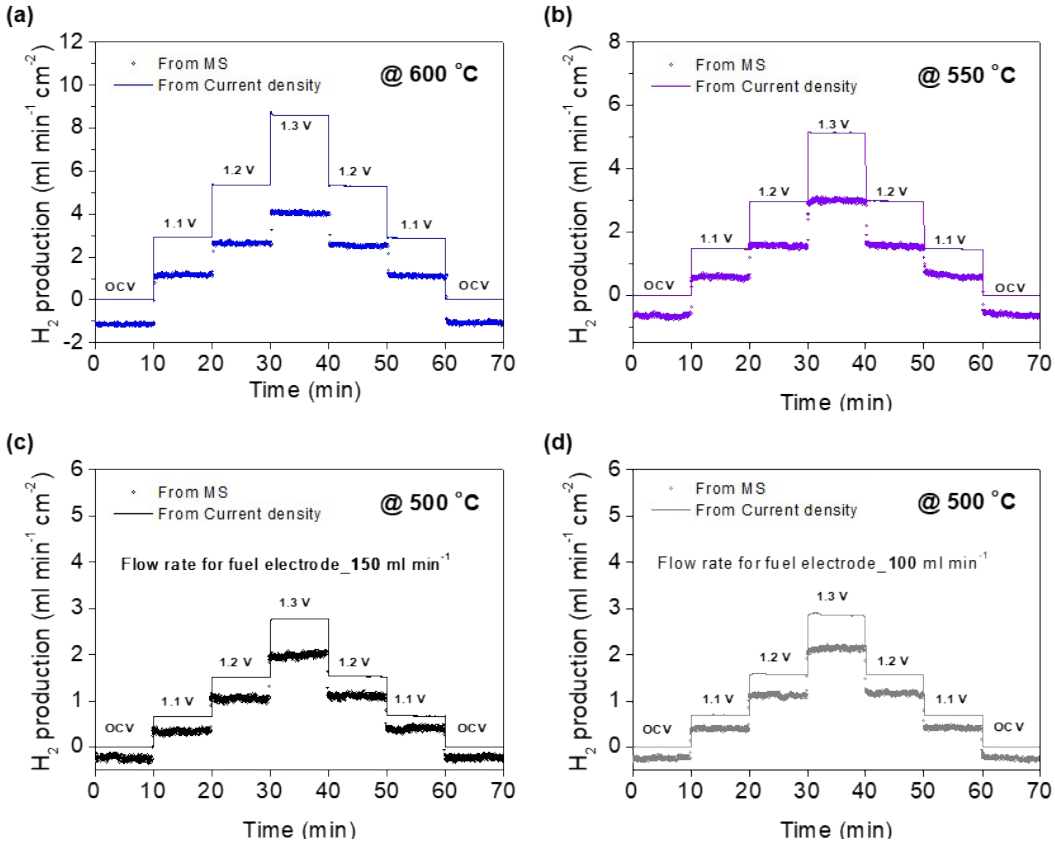

Figure S6. A trace of hydrogen detected under different voltage conditions. Hydrogen production rate by converting from the current density (line) and directly measuring from the MS (dot) at (a) 600, (b) 550, and (c) 500 °C. (d) Reduced flow rate (100 ml min^{-1}) is used at fuel electrode side at 500 °C to check the possible mechanical leaks across the cell or through the apparatus.

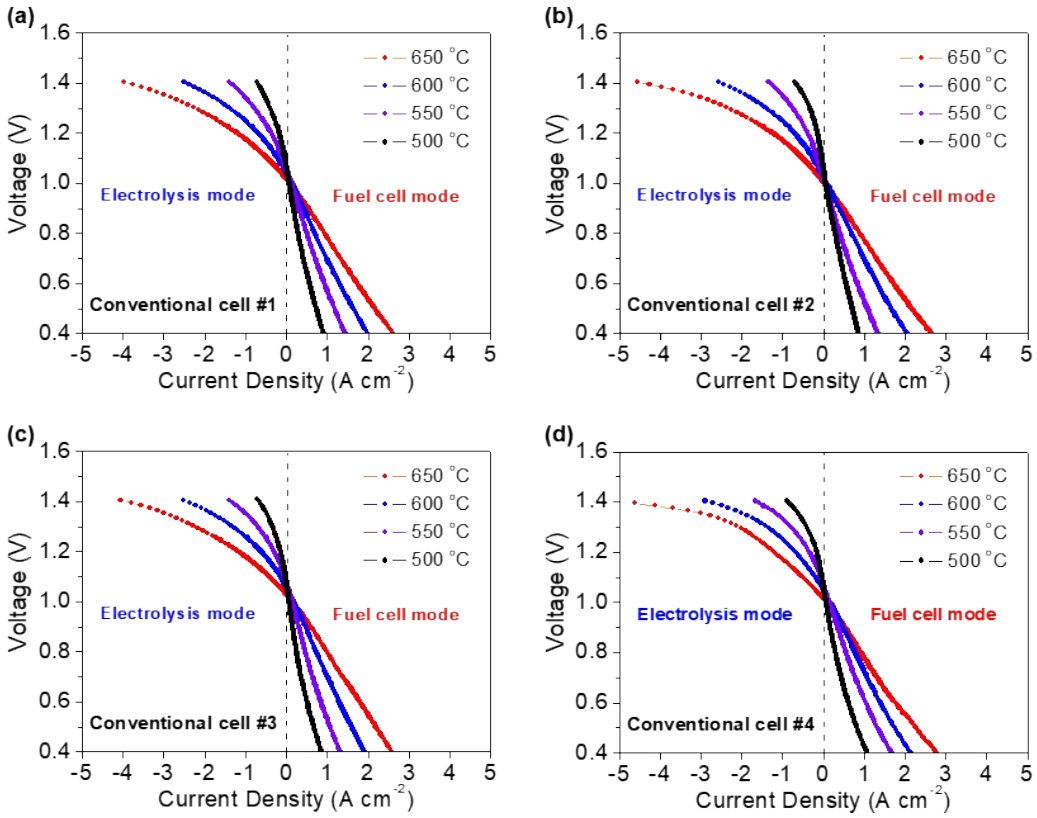

Figure S7. IV curves of all measurements with conventional cells under humidified (3 % H_2O) H_2 and (3 % H_2O) air. The conventional Cell #1 is used to attain the IV curve, corresponded power density, and long term hydrogen evolution as shown in the main text in Fig. 3a, b, and d. Conventional cell #2 is used to obtain reversible cycling operation in Fig. 3c. The average performance values for electrolysis mode (current density at 1.3 V) and fuel cell mode (peak power density) are summarized with standard deviation in Fig. 6.

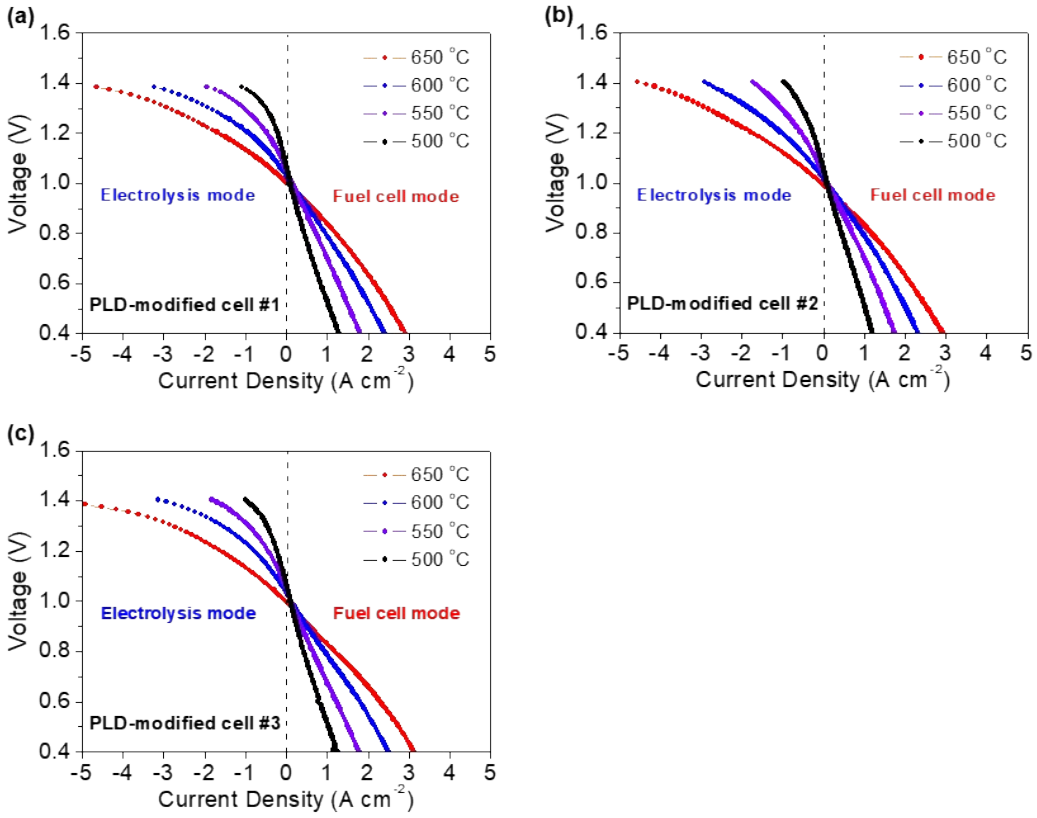

Figure S8. IV curves of all measurements with PLD modified cells under humidified (3 % H_2O) H_2 and (3 % H_2O) air. The PLD-modified cell #1 is used to perform the electrochemical characterization with long-term stability measurement in Fig. 5. The average performance values for electrolysis mode (current density at 1.3 V) and fuel cell mode (peak power density) are summarized with standard deviation in Fig. 6.

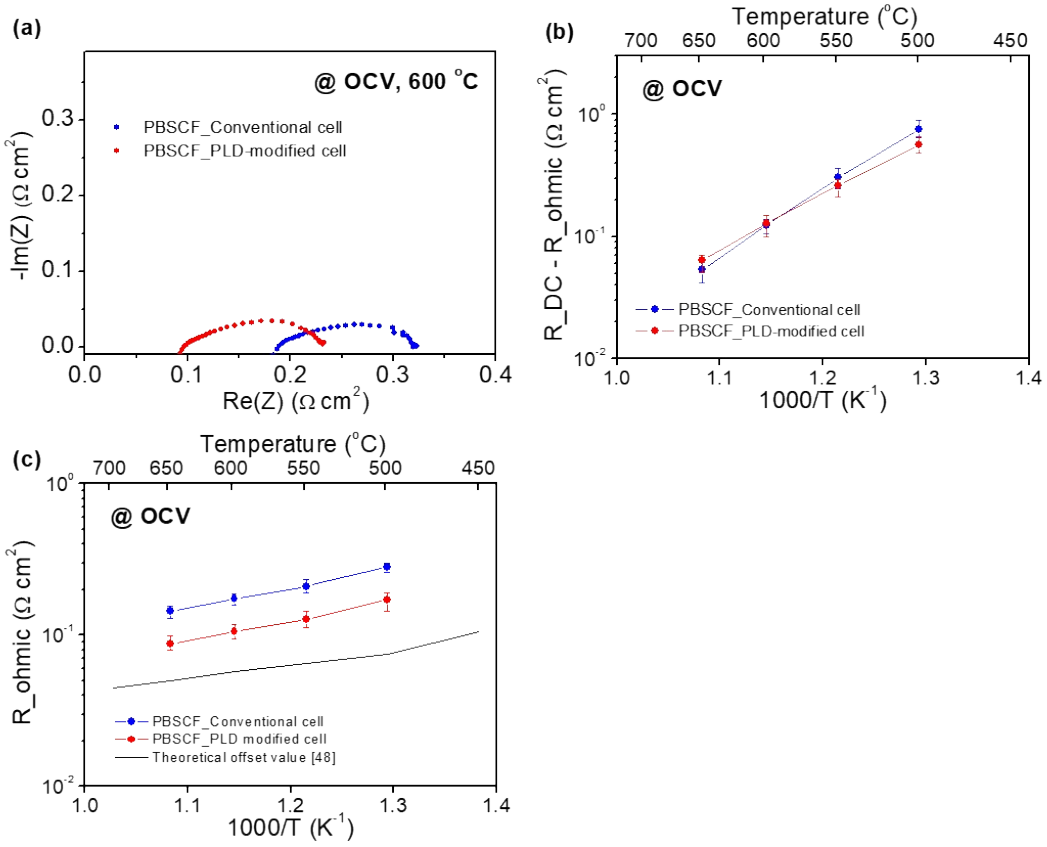

Figure S9. The impact of additional PLD layer on electrochemical resistance. (a) Impedance spectra of conventional and PLD-modified cells under OCV condition at 600 °C (b) R_DC – R_ohmic resistance of conventional and PLD-modified cells under open circuit condition. (c) Comparison of the offset (ohmic) resistances of conventional and PLD-modified cells as measured by impedance spectroscopy at open circuit conditions

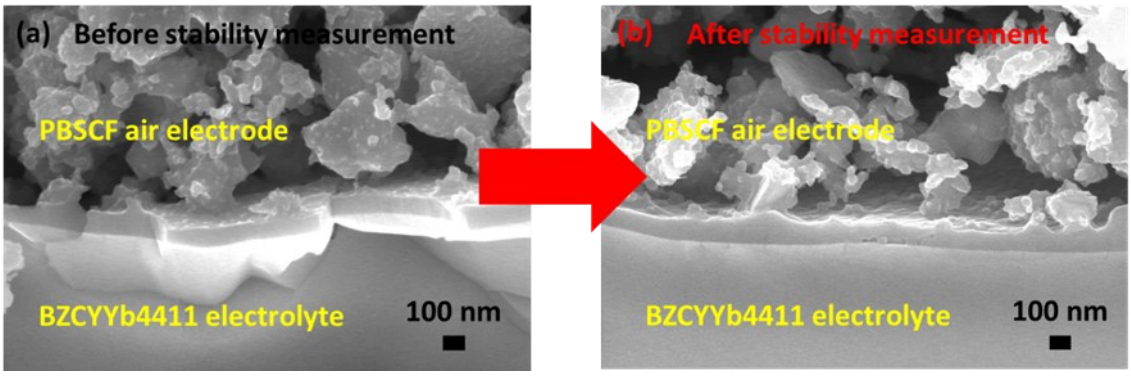

Figure S10. Absence of microstrucural changes during stability measurement with PLD-modified cell. Microstructure of interface at PBSCF air electrode and BZCYYb4411 electrolyte with inserted additional PBSCF PLD layer (a) before and (b) after stability measurement under electrolysis operation (1.3 V) at 550 ^{o}C as shown in Fig. 5b.

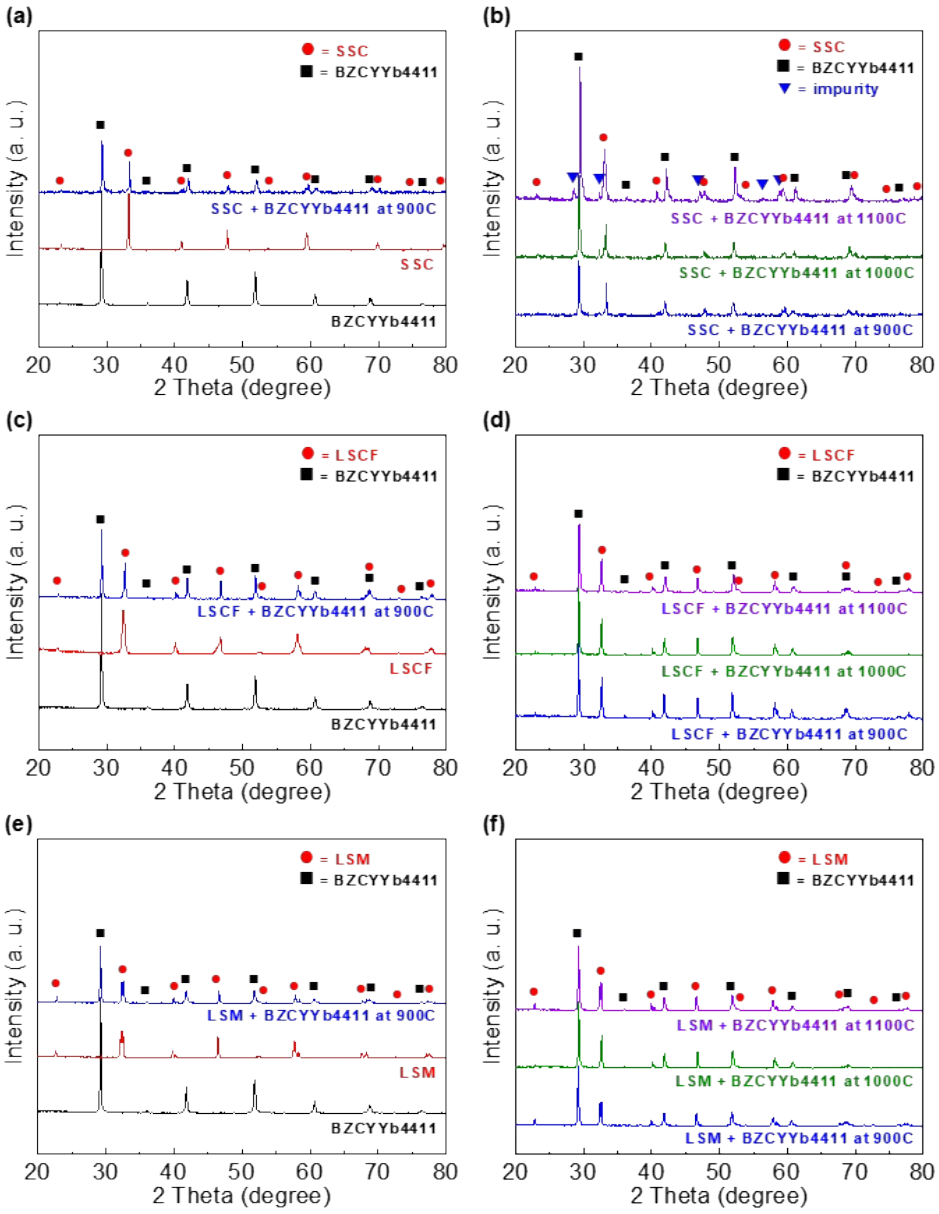

Figure S11. Chemical compatibility between various air electrodes and BZCYYb4411 electrolyte. X-ray diffraction (XRD) patterns for sintered BZCYYb4411 and (a and b) SSC, (c and d) LSCF, and (e and f) LSM air electrodes are shown as references for the diffraction pattern, and a mixture of the two materials annealed at 900, 1000, and 1100 °C under air. In SSC, XRD patterns indicate that there occurs impurities after annealing process as shown in b. There is no detectable secondary phases with LSCF and LSM after heat treatment.

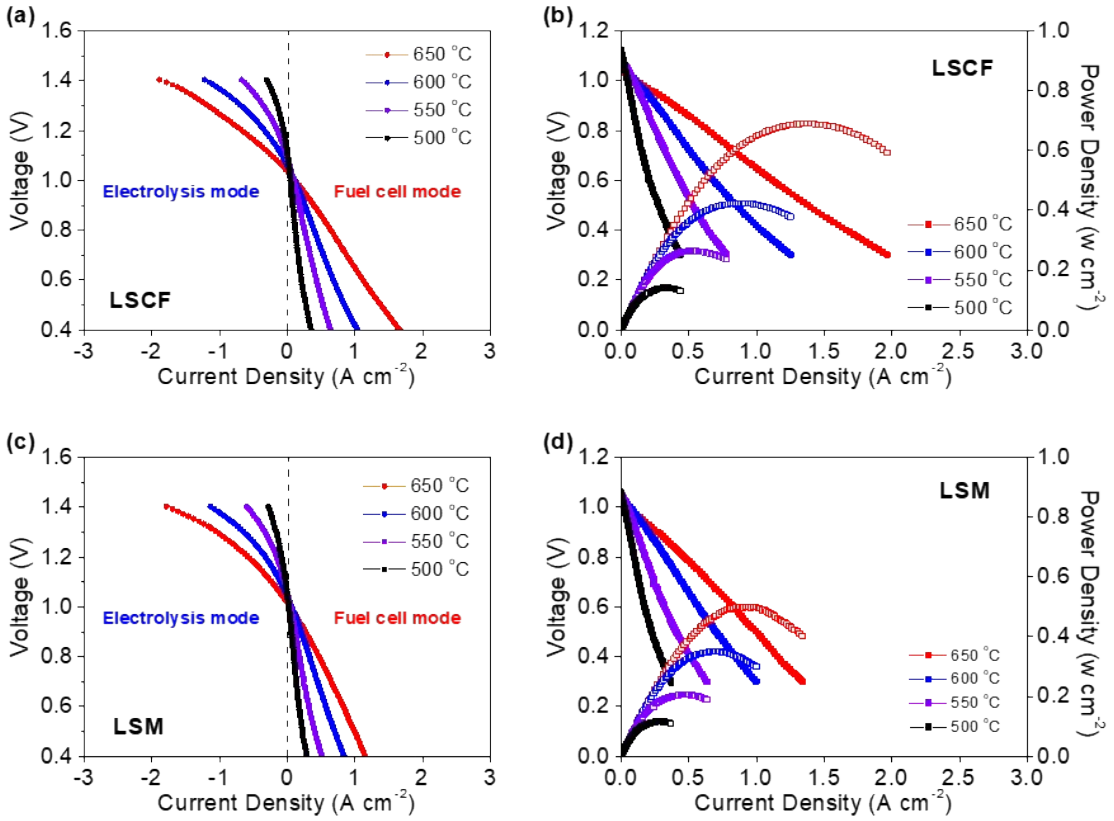

Figure S12. Electrochemical performance of alternative air electrodes. (a) IV curves and (b) polarization and power density curves for fuel cell mode with LSCF air electrode based on BZCYYb4411 electrolyte using conventional cells in humidified (3 % H_2O) H_2 and (3 % H_2O) air. (c) IV curves and (d) polarization and power density curves for fuel cell mode with LSM air electrode

Table S1. Performance of electrolysis cells based on an oxygen ion (O^{2-}) conducting electrolyte

Ref.	Cell configuration (Air electrode/Electrolyte (Thickness)/ Fuel electrode)	Inlet Gas composition		Temp (°C)	OCV (V)	Current density @ 1.3V (A cm^{-2})
		For Air electrode	For fuel electrode			
(20)	PBSCF-GDC/LSGM (250 μm)/ LDC/PBM(Co-Fe)	Air	H_2 (10 % H_2O)	800 700	1.00 1.05	-1.31 -0.52
(21)	LSCF-GDC/GDC/YSZ (7 μm)/ Ni-YSZ	Air	H_2 (50 % H_2O)	750	0.94	-2.10
(22)	BLC/LSGM (300 μm)/ CMF	Air	1 % H_2 +79 % Ar (20 % H_2O)	800 700	0.78 0.85	-0.37 -0.10
(23)	LSM-YSZ/LNWO (360 μm)/ Ni-YSZ	20 % O_2 + 80 % N_2	H_2 (50 % H_2O)	950 850	0.91 0.96	-0.26 -0.04
(27)	PNO/PNO-CGO/YSZ (20 μm)/ Ni-YSZ	Ambient air	H_2 (50 % H_2O)	800	0.94	-0.78
(28)	NNO-SSZ/SSZ (12 μm)/ Ni-SSZ	Air	H_2 (50 % H_2O)	800 700	0.94 0.99	-1.08 -0.44
(29)	LSCF/LSCF-GDC/GDC/YSZ (20 μm)/ /Ni-YSZ	Air	H_2 (50 % H_2O)	800	1.10	-0.85
(30)	LSM-YSZ/YSZ (13 μm)/ Ni-YSZ	Ambient air	H_2 (50 % H_2O)	750	1.00	-1.42
(31)	LSCF-SDC/LSGM (n/a)/ LCO/SFMNi-SDC	Ambient air	H_2 (42 % H_2O)	800 700	0.92 0.93	-0.84 -0.27
(32)	LSM-YSZ/YSZ (10 μm)/ Ni-YSZ	Ambient air	H_2 (33 % H_2O)	800	0.87	-1.35
(33)	LSM-YSB/YSZ (10 μm)/ Ni-YSZ	100 % O_2	H_2 (45 % H_2O)	800	0.98	-1.52
(34)	LSCF/LSGM (n/a)/ Ni-LSGM/SLT	Air	H_2 (50 % H_2O)	600	1.00	-0.92

For air electrode

PBSCF = $PrBa_{0.5}Sr_{0.5}Co_{1.5}Fe_{0.5}O_{5+\delta}$; LSCF = $La_{0.6}Sr_{0.4}Co_{0.2}Fe_{0.8}O_{3-\delta}$; BLC = $Ba_{0.6}La_{0.4}CoO_{3-\delta}$; LSM = $(La_{0.8}Sr_{0.2})_{0.98}MnO_{3-\delta}$; PNO=$Pr_2NiO_{4+\delta}$; NNO = $Nd_2NiO_{4+\delta}$;

For electrolyte

GDC or CGO = gadolinium doped ceria, $Ce_{0.9}Gd_{0.1}O_{2-\delta}$; LSGM= $La_{0.9}Sr_{0.1}Ga_{0.8}Mg_{0.2}O_{3-\delta}$; LDC= $La_{0.4}Ce_{0.6}O_{2-\delta}$; YSZ= yttria-stabilized zirconia; LNWO = $LaNb_{0.84}W_{0.16}O_{4.08}$; SSZ = Scandia stabilized zirconia; SDC = $Sm_{0.2}Ce_{0.8}O_{1.9}$; LCO = $La_{0.5}Ce_{0.5}O_{1.5}$; YSB=$Bi_{0.42}Y_{0.58}O_{1.5}$;

For fuel electrode

PBM= $PrBaMn_2O_{5+\delta}$; CMF= $Ce_{0.6}Mn_{0.3}Fe_{0.1}O_{2-\delta}$; SFMNi = $Sr_2Fe_{1.3}Ni_{0.2}Mo_{0.5}O_6$; SLT = $Sr_{0.8}La_{0.2}TiO_{3-\delta}$;

n/a = not available

Table S2. High-temperature performance of electrolysis cells based on a proton conducting (H^+) electrolyte

Ref.	Cell configuration (Air electrode/Electrolyte (Thickness)/ Fuel electrode)	Inlet Gas composition		OCV/E_N (V)	Current density @ 1.3V (A cm^{-2})	Faraday Efficiency @ 1.3V (%)
		For air electrode	For fuel electrode			
700C						
(35)	SSC/BZCY44(1500 μm)/ Pt	Air (20 % H_2O)	5 % H_2/Ar (3 % H_2O)	0.95/0.96	-0.035	> 80
(42)	NBSCF-BZCYYb1711/BZCYYb1711 (20 μm)/ Ni-BZCYYb1711	Air (10 % H_2O)	H_2 (10 % H_2O)	1.00/1.00	-2.41	n/a
(43)	LSCM-BZCYZ/BCZYZ (75 μm)/ Ni-BCZYZ	N_2 (3 % H_2O)	5 % H_2 + 95 % Ar	0.13	-0.96	22 @ 2.0V
(45)	$LSMS_{0.05}$/BCZYZ (2000 μm)/ $LSMS_{0.05}$	Air (5 % H_2O)	5 % H_2 + 95 % Ar	0.60/1.05	-0.022	80 @ 2.0V
800C						
(44)	LSCF-BZCYZ/BCZYZ (2000 μm)/ Ni-BCZYZ	Air (3 % H_2O)	5 % H_2 + 95 % Ar	0.75/0.97	-0.03 @ 1.4V	37.5 @ 1.4V
(44)	BSCF-BZCYZ/ BCZYZ (2000 μm)/ Ni-BCZYZ	Air (3 % H_2O)	5 % H_2 + 95 % Ar	0.73/0.97	-0.03 @ 1.4V	43.8 @ 1.4V
(46)	6 wt% Co_3O_4-LSM-BCZYZ/ BCZYZ (2000 μm)/Ni-BCZYZ	Air (10 % H_2O)	5 % H_2 + 95 % Ar	0.92/0.94	-0.07 @ 1.4V	43.3 @ 1.4V

For air electrode

LSCM = $La_{0.75}Sr_{0.25}Cr_{0.5}Mn_{0.5}O_{3-d}$; NBSCF = $NdBa_{0.5}Sr_{0.5}Co_{1.5}Fe_{0.5}O_{5+d}$; SSC = $Sm_{0.5}Sr_{0.5}CoO_{3-d}$; $LSMS_{0.05}$ = $La_{0.8}Sr_{0.2}Mn_{0.95}Sc_{0.05}O_{3-d}$; LSCF = $La_{0.6}Sr_{0.4}Co_{0.2}Fe_{0.8}O_{3-d}$; BSCF = $Ba_{0.5}Sr_{0.5}Co_{0.8}Fe_{0.2}O_{3-d}$; LSM = $La_{0.8}Sr_{0.2}MnO_{3-d}$

For electrolyte

BCZYZ = $BaCe_{0.5}Zr_{0.3}Y_{0.16}Zn_{0.04}O_3$; BZCYYb1711 = $BaZr_{0.1}Ce_{0.7}Y_{0.1}Yb_{0.1}O_3$; BZCY44 = $BaCe_{0.4}Zr_{0.4}Y_{0.2}O_3$; BZY20 = $BaZr_{0.8}Y_{0.2}O_3$; BCZD = $BaCe_{0.5}Zr_{0.3}Dy_{0.2}O_3$; BCZY = $BaCe_{0.5}Zr_{0.3}Y_{0.2}O_3$; BZY10 = $BaZr_{0.9}Y_{0.1}O_3$; BZCYYb1711 = $BaZr_{0.1}Ce_{0.7}Y_{0.1}Yb_{0.1}O_3$; BZCYYb4411 = $BaZr_{0.4}Ce_{0.4}Y_{0.1}Yb_{0.1}O_3$

n/a = not available

Table S3. Electrochemical characteristics of representative protonic ceramic electrochemical cells under open circuit conditions: V_N is the computed Nernst voltage; V_{OC}, R_{ohmic}, and R_{DC} are measured values of, respectively, the open circuit voltage, the high frequency resistance, and the resistance in the low frequency limit; R_{e^-}, R_{H^+}, R_P, and $I_{H^+}^{OC}$ are, respectively, the computed electronic resistance, protonic resistance, polarization resistance, and ionic leakage current. Cells are measured with 97 % hydrogen, balance steam, supplied to the fuel electrode and 3 % H_2O humidified synthetic air supplied to the air electrode.

T, °C	V_N, V	V_{OC}, V	R_{ohmic}, Ωcm^2	R_{DC}, Ωcm^2	R_{e^-}, Ωcm^2	R_{H^+}, Ωcm^2	t_{H^+}	R_P, Ωcm^2	$I_{H^+}^{OC}$, Acm^{-2}	$\eta_F^{1.3V}$ (%)	$I_{H^+}^{1.3V}$, Acm^{-2}
Conventional cell #1											
650	1.07	1.02	0.15	0.20	4.05	0.16	0.96	0.05	0.25	77	-1.74
600	1.08	1.05	0.18	0.32	10.2	0.19	0.98	0.14	0.10	84	-1.18
550	1.10	1.07	0.22	0.47	19.6	0.22	0.99	0.25	0.06	86	-0.67
500	1.11	1.08	0.30	0.94	38.7	0.30	0.99	0.66	0.03	87	-0.33
PLD-modified cell #1											
650	1.07	1.01	0.08	0.15	2.55	0.08	0.97	0.08	0.40	74	-2.15
600	1.08	1.03	0.10	0.23	4.62	0.10	0.98	0.15	0.22	76	-1.37
550	1.10	1.06	0.11	0.40	12.1	0.13	0.99	0.28	0.09	81	-0.83
500	1.11	1.07	0.14	0.80	23.8	0.15	0.99	0.68	0.05	82	-0.42

Application of a PLD layer largely improves the electronic contact between air electrode and the electrolyte, as reflected in the decrease of R_{e^-}, although a slightly improvement in the protonic contact is also observed. As a consequence, both the electronic and ionic currents increase. The transference number is unchanged, as would be expected, as is the electrochemical reaction resistance, implying that the PLD layer does not impact the redox reaction, as also expected. Despite a slight penalty in Faradaic efficiency upon PLD-modification, because of the overall decrease in cell resistance terms, the hydrogen production rate increases at any given voltage. This behavior is exemplified by the tabulated data for an operating voltage 1.3 V.

References

1. M. P. Pechini US Patent 1967, 3, 330, 697.
2. W. Lai, S. M. Haile, *Phys. Chem. Chem. Phys.*, 2008, **10,** 865-883.
3. M. Liu and H. Hu, *J. Electrochem. Soc.* 1996, **143(6),** L109-L112.